PERGAMON

International Journal of Rock Mechanics and Mining Sciences 37 (2000) 121–132

International Journal of
Rock Mechanics
and Mining Sciences

www.elsevier.com/locate/ijrmms

Frictional effects on the volumetric strain of sandstone

K.T. Nihei[a,*], L.B. Hilbert Jr[b], N.G.W. Cook[a], S. Nakagawa[a], L.R. Myer[a]

[a]*Earth Sciences Division, Lawrence Berkeley National Laboratory, 1 Cyclotron Road, MS 90-1116, Berkeley, CA 94720, USA*
[b]*Exponent, 149 Commonwealth Drive, Menlo Park, CA 94025, USA*

Accepted 7 October 1999

Abstract

The contributions of frictional slip on the nonlinear, hysteretic deformation of sandstone in the reversible regime (i.e., prior to the onset of permanent deformation) for uniaxial strain compression are investigated through an analysis of a Hertz–Mindlin face-centered cubic sphere pack model and laboratory stress–strain tests on Berea sandstone. The analysis demonstrates that the dynamic[1] moduli are path-independent functions of the strain. The analysis also reveals that for uniaxial strain consolidation it is possible to decompose the volumetric strain into a path-independent contribution from nonlinear grain contact deformation and a path-dependent contribution from frictional (slip) compaction. Laboratory stress–strain measurements on Berea sandstone support these findings and, in addition, reveal that frictional compaction accounts for a significant portion of the volumetric strain of Berea sandstone.

1. Introduction

Sandstones represent a class of granular materials that can exhibit complex stress–strain characteristics such as nonlinearity, hysteresis and stress-induced anisotropy when subjected to compressive stresses, even for stresses well below the uniaxial compressive strength where the mechanical behavior is largely reversible (i.e., where there is no permanent strain after the sample is unloaded). These characteristics result largely from nonlinear deformation and frictional slip at the grain contacts.

While the contribution of frictional slip to the volumetric strain of granular materials such as soils and sediments is well-recognized in soil mechanics, there are fewer studies in the field of rock mechanics describing the role of friction on the deformation of more competent granular materials such as sandstones (e.g. [4,11,14,23]). Many investigations of the compressibility of sandstones are still based on the assumptions that the rock is isotropic and elastic. In the earth where deviatoric stresses are the norm, granular rocks such as sandstones typically exhibit nonlinear, hysteretic deformation.

The paper begins with a general overview of the effects of anisotropy and nonlinearity on the volumetric strain of rock which illustrates some of the deficiencies of existing models. This overview is followed by an analysis of the stress–strain characteristics of a face-centered cubic (fcc) sphere pack subjected to uniaxial strain loading. This analysis demonstrates how the volumetric strain can be decomposed into contributions from intergranular frictional slip and nonlinear grain contact deformation. This decomposition is then applied to uniaxial strain stress–strain data for Berea sandstone to estimate the frictional contribution to the volumetric strain. The final section summarizes the basic findings of this study.

* Corresponding author. Tel.: +1-510-486-5349; fax: +1-510-486-5686.

E-mail address: ktnihei@lbl.gov (K.T. Nihei).

[1] Throughout this paper the term *dynamic* moduli will be used to denote the small-strain tangent moduli for conditions where there is no frictional slip between grains. Linear elastic waves are generally assumed to propagate with wave speeds computed from the dynamic moduli.

1365-1609/00/$ - see front matter
PII: S1365-1609(99)00098-2

2. Review of linear, nonlinear, and hysteretic deformation of rock

When a granular rock such as sandstone is subjected to compressive stresses, the pore volume is reduced by the deformation of the solid grains and closure of the compliant portions of the pore space. The total volume of the rock (V_b) is related to the volume of the grains (V_r) and pores (V_p) through the relation, $V_b = V_r + V_p$. The (bulk) volumetric strain is defined as the change in volume over the initial volume

$$\varepsilon_b = \frac{\Delta V_b}{V_b^i}. \tag{1}$$

The volumetric strain can be expressed in terms of components of the strain tensor ε_{ij} by decomposing the strain tensor into its spherical and deviatoric parts,

$$\varepsilon_{ij} = \tfrac{1}{3}\varepsilon_{kk}\delta_{ij} + (\varepsilon_{ij} - \tfrac{1}{3}\varepsilon_{kk}\delta_{ij}) \equiv \text{spherical} + \text{deviatoric}. \tag{2}$$

The deviatoric strain provides a measure of the change in shape of the rock, while the spherical part provides a measure of the change in volume (i.e., the bulk volumetric strain),

$$\varepsilon_b = \tfrac{1}{3}\varepsilon_{ij}\delta_{ij} + O(\varepsilon^2) \cong (\varepsilon_{11} + \varepsilon_{22} + \varepsilon_{33}). \tag{3}$$

For an anisotropic linear elastic solid, the volumetric strain is related to the stresses which produced it through a contraction on the i index of the fourth-rank elastic compliance tensor s_{ijkl},

$$\varepsilon_b = s_{iikl}\sigma_{kl}, \tag{4}$$

or in a condensed notation,

$$\varepsilon_b = s_{IJ}\sigma_J, \tag{5}$$

where $I = 1, 2, 3$ and $J = 1, \ldots, 6$. s_{IJ} is the 3×6 compliance tensor of the anisotropic compressibilities,

$$s_{IJ} = \begin{cases} s_{iikl}, & J = 1, 2, 3 \\ s_{iikl}/2, & J = 4, 5, 6 \end{cases}, \tag{6}$$

and σ_J is the 6×1 stress tensor $\sigma_J = [\sigma_{11}, \sigma_{22}, \sigma_{33}, \sigma_{23}, \sigma_{13}, \sigma_{12}]^T$. From Eq. (5), it is easy to show that for general anisotropy the volumetric strain of the rock results from a combination of normal and shear stresses. However, if the rock is of orthorhombic symmetry or higher and the symmetry axes aligned with the normal stress directions, then the volumetric strain will depend only on the normal stresses. In general, the volumetric strain of a rock will not solely be a function of the *mean* or average stress, even for rocks exhibiting linear elastic stress–strain behaviors, unless the rock is isotropic.

For the special case of isotropy, Eq. (5) takes the simple form

$$\varepsilon_b = (1/K)\bar{\sigma} = S\bar{\sigma}, \tag{7}$$

where S is the bulk compressibility of the rock when subjected to confining stresses, K is the bulk modulus of the rock, and $\bar{\sigma} = (\sigma_1 + \sigma_2 + \sigma_3)/3$ is the *mean* or average stress. It should be noted that, to date, much of the research on the compressibility of rock is based on the assumption of isotropy for which the compressibility is a scalar quantity (e.g. [27,28]). Eq. (7) can be modified to describe the bulk strain of a nonlinear rock by replacing the stress and strain with their differentials and allowing the compressibility to be stress-dependent [28],

$$\mathrm{d}\varepsilon_b = S(\bar{\sigma})\mathrm{d}\bar{\sigma}. \tag{8}$$

Use of this integrated stress–strain relation to capture the nonlinearity of rock is strictly valid provided the initially isotropic rock retains its isotropy as it is compressed. Since many rocks exhibit stress-induced anisotropy and hysteresis when subjected to non-hydrostatic stresses [15–17,22], the integrated form, Eq. (8), should only be used for isotropic loading (i.e., hydrostatic stresses).

For non-hydrostatic states of stress, only a limited number of nonlinear elasticity models which are capable of predicting stress-induced anisotropy have been developed. For example, the third-order hyperelastic model (based on the assumption that the strain energy density function is a third-order polynomial) have been used extensively to model the behavior of soils (e.g., see [1]) and, recently, rock [9,10,15,18]. The third-order hyperelastic model for a non-prestressed, initially isotropic solid is described by five constants. This model is capable of predicting path-independent stress-induced anisotropy and shear-dilatancy,

$$\varepsilon_b = \left[\frac{1}{K} + 9\bar{\sigma}(9d_4 + d_5)\right]\bar{\sigma} + \left(\frac{3d_5}{2} + d_6\right)(\sigma_1^2 + \sigma_2^2 + \sigma_3^2) + (3d_5 + 2d_6)(\sigma_4^2 + \sigma_5^2 + \sigma_6^2), \tag{9}$$

where K is a second-order elastic constant, and d_4, d_5, and d_6 are the third-order elastic constants. The first term in Eq. (9) is dependent only on the mean stress. The second term is a function of the squares of the normal stresses, resulting in nonlinearity in the bulk strain versus normal stress relation. The third term is a nonlinear function of the shear stresses, offering the possibility of shear-dilation or shear-compaction. The primary limitation of Eq. (9) when applied to sandstones is that its path-independent nature precludes it from including hysteresis resulting from frictional slip between grains (e.g., see [16,21]). Hypoelastic models offer the possibility of including path-dependence by adopting a formulation in which the stress-rate is a function of the current strain-state and strain-rate.

However, these models offer little insight into the physics producing the path-dependence and can amount to a curve fitting exercise with up to 21 material moduli for general triaxial loading [1].

Currently, there are no general analytic models of granular rock which include both nonlinearity and frictional slip. Closed-form expressions for the stress–strain behavior of random sphere packs have been derived by Walton [26], Norris and Johnson [21] and Johnson et al. [16] for the particular cases of smooth contacts with reversible slip and frictionally-locked contacts. While these models predict stress-induced anisotropy, path-dependent stress–strain relationships, and path-independent second-order elastic moduli (i.e., wave speeds), they do not allow for general frictional behavior where the grains may experience frictional slip and lock-up during the course of loading, unloading, and reloading of the material. Consequently, these models do not predict differences between the static (tangent) and dynamic moduli[1], a behavior which is commonly observed in granular media such as sediments and sandstones (e.g. [13]). Other analytic models of the frictional deformation of random packings of grains have been presented (e.g. [2]), but several of these models have recently been demonstrated to be based on non-physical contact force laws [8].

There are a number of closed-form analytic solutions for the stress–strain behaviors of regular packings of identical spheres (e.g., simple cubic, face-centered cubic, hexagonal close packed) that were developed by Mindlin and others [5–7,25]. These models have the disadvantage of lacking grain packing disorder, grain angularity, and intergranular cementation that are prevalent in most sandstones. However, because these models do include the contributions of grain contact nonlinearity and frictional slip to the volumetric strain, they represent a logical starting point for the investigation of the effects of friction on the nonlinear, hysteretic deformation of sandstones.

3. Volumetric strain of an FCC sphere pack for uniaxial strain loading

To examine the contribution of frictional slip to the volumetric strain of granular rock, we will use the face-centered cubic packing (fcc) model of spheres of identical size and properties. This model is one of the densest regular arrays of elastic spheres with a porosity of 25.95% and a coordination number of 12 (Fig. 1). Both the effects of Hertzian grain contact deformation and Mindlin-type intergranular slip [19] are included in the model.

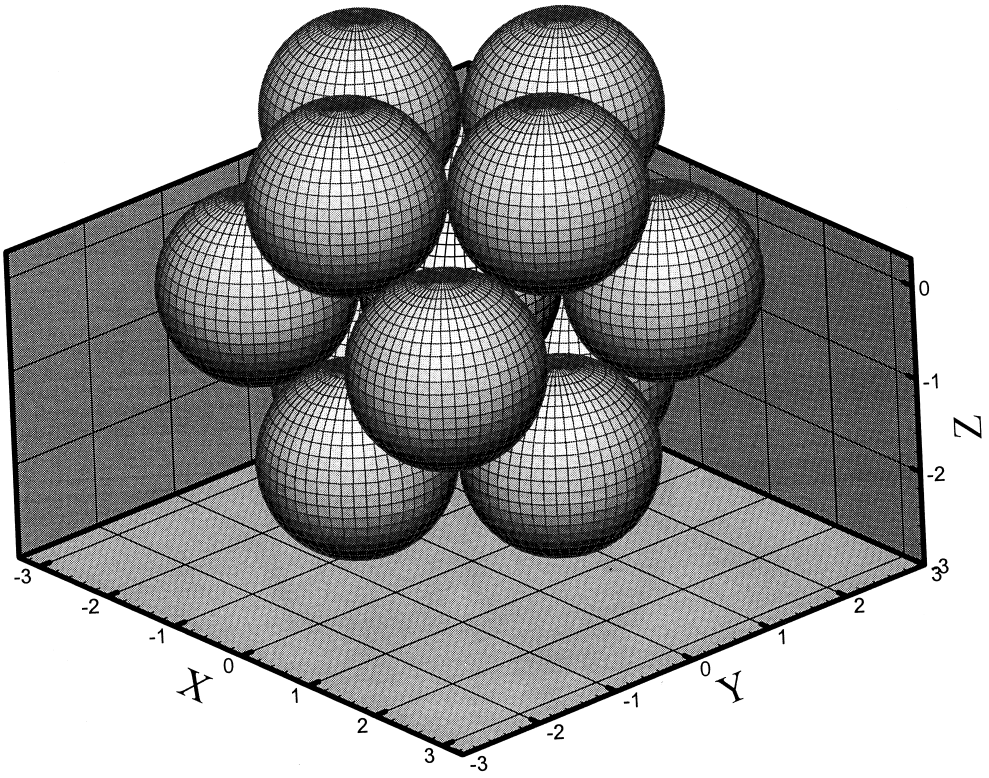

Fig. 1. Schematic of a face-centered cubic (fcc) packing of identical elastic spheres (porosity = 25.95%, coordination number = 12). Nonlinear deformation and frictional slip at the grain contacts are described by Hertz–Mindlin contact mechanics for elastic spheres.

3.1. Stress–strain relations for uniaxial strain

The differential stress–strain relations for the fcc packing subjected to axisymmetric loading along the z-axis are those for a medium with tetragonal symmetry [7],

$$\begin{bmatrix} d\sigma_{xx} \\ d\sigma_{yy} \\ d\sigma_{zz} \\ d\sigma_{yz} \\ d\sigma_{zx} \\ d\sigma_{xy} \end{bmatrix} = \begin{bmatrix} c_{11} & c_{12} & c_{13} & 0 & 0 & 0 \\ c_{12} & c_{11} & c_{13} & 0 & 0 & 0 \\ c_{13} & c_{13} & c_{33} & 0 & 0 & 0 \\ 0 & 0 & 0 & 2c_{44} & 0 & 0 \\ 0 & 0 & 0 & 0 & 2c_{44} & 0 \\ 0 & 0 & 0 & 0 & 0 & 2c_{66} \end{bmatrix} \begin{bmatrix} d\varepsilon_{xx} \\ d\varepsilon_{yy} \\ d\varepsilon_{zz} \\ d\varepsilon_{yz} \\ d\varepsilon_{zx} \\ d\varepsilon_{xy} \end{bmatrix} \tag{10}$$

where c_{IJ} are the elastic constants. The corresponding strain–stress relations are

$$\begin{bmatrix} d\varepsilon_{xx} \\ d\varepsilon_{yy} \\ d\varepsilon_{zz} \\ d\varepsilon_{yz} \\ d\varepsilon_{zx} \\ d\varepsilon_{xy} \end{bmatrix} = \begin{bmatrix} s_{11} & s_{12} & s_{13} & 0 & 0 & 0 \\ s_{12} & s_{11} & s_{13} & 0 & 0 & 0 \\ s_{13} & s_{13} & s_{33} & 0 & 0 & 0 \\ 0 & 0 & 0 & s_{44} & 0 & 0 \\ 0 & 0 & 0 & 0 & s_{44} & 0 \\ 0 & 0 & 0 & 0 & 0 & s_{66} \end{bmatrix} \begin{bmatrix} d\sigma_{xx} \\ d\sigma_{yy} \\ d\sigma_{zz} \\ d\sigma_{yz} \\ d\sigma_{zx} \\ d\sigma_{xy} \end{bmatrix} \tag{11}$$

where s_{IJ} are the elastic compliances. For one-dimensional consolidation (i.e., uniaxial strain loading) along the z-axis, all the strains are zero except $d\varepsilon_{zz}$. Thus, the volumetric strain for this state of stress is

$$d\varepsilon_b \equiv d\varepsilon_{zz} = 2s_{13}\, d\sigma_{xx} + s_{33}\, d\sigma_{zz}, \tag{12}$$

where, in general, $s_{13} \neq s_{33}$, indicating that the volumetric strain is not solely a function of the mean stress.

Hendron [12] and Stoll [24] used the results from Duffy and Mindlin [7] for the fcc packing and Mindlin and Deresiewicz [20] for determining the tangential compliances of contacting spheres to develop explicit (i.e., total) stress–strain equations for uniaxial strain loading. This particular state of stress has the benefits of the strain being a scalar (i.e., $\varepsilon_b = \varepsilon_{zz}$), and, additionally, it corresponds to the state of stress produced by elastic waves in the earth and in laboratory samples with dimensions that are larger than the seismic wavelength.

The stress–strain relation for the initial loading path $0 \rightarrow A$, as shown in Fig. 2 [12], is

$$\sigma_{zz}^{\text{load}} = \left[\frac{2\mu}{3(1-\nu)}\right](1+f)\varepsilon_{zz}^{3/2}, \tag{13}$$

where μ and ν are the shear modulus and Poisson's ratio of the grains, respectively, and f is the intergranular coefficient of fraction. The stress–strain relations for the unloading path $A \rightarrow B$, as shown in Fig. 2, are [24]

$$\sigma_{zz}^{\text{unload}} = \left[\frac{2\mu}{3(1-\nu)}\right]\{(1-f)\varepsilon_{zz}^{3/2} + 2f[(1+K_2)\varepsilon_{zz}^{*} - K_2\varepsilon_{zz}]^{3/2}\}, \quad \text{for } [(1+K_2)\varepsilon_{zz}^{*} - K_2\varepsilon_{zz}] \geq 0 \tag{14a}$$

$$\sigma_{zz}^{\text{unload}} = \left[\frac{2\mu}{3(1-\nu)}\right](1-f)\varepsilon_{zz}^{3/2}, \quad \text{for } [(1+K_2)\varepsilon_{zz}^{*} - K_2\varepsilon_{zz}] < 0, \tag{14b}$$

where $K_2 = -(1+K_1 f)/(2K_1 f)$, $K_1 = (2-\nu)/[2(1-\nu)]$, and ε_{zz}^{*} is the strain at the point of unloading. The stress–strain relations for the reloading path $B \rightarrow C$, as shown in Fig. 2, are (Appendix)

$$\sigma_{zz}^{\text{reload}} = \left[\frac{2\mu}{3(1-\nu)}\right]\{(1+f)\varepsilon_{zz}^{3/2} + 2f[(1+K_2)\varepsilon_{zz}^{*} - K_2\varepsilon_{zz}^{**}]^{3/2} - 2f[(1+K_3)\varepsilon_{zz}^{**} - K_3\varepsilon_{zz}]^{3/2}\}, \quad \text{for } [(1+K_2)\varepsilon_{zz}^{*} - K_2\varepsilon_{zz}^{**}] \geq 0 \tag{15a}$$

$$\sigma_{zz}^{\text{reload}} = \left[\frac{2\mu}{3(1-\nu)}\right]\{(1+f)\varepsilon_{zz}^{3/2} - 2f[(1+K_3)\varepsilon_{zz}^{**} - K_3\varepsilon_{zz}]^{3/2}\}, \quad \text{for } [(1+K_2)\varepsilon_{zz}^{*} - K_2\varepsilon_{zz}^{**}] < 0 \tag{15b}$$

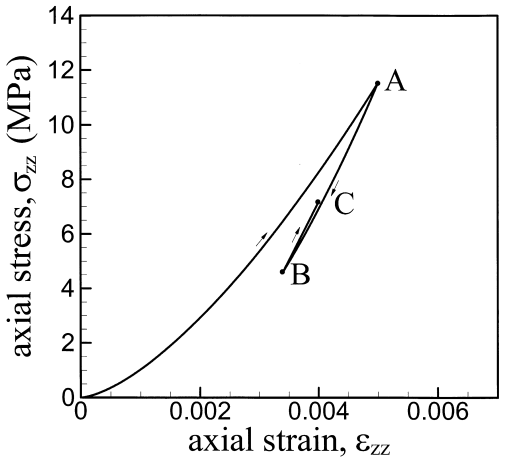

Fig. 2. Computed σ_{zz} vs ε_{zz} curve for the fcc packing under uniaxial strain conditions. The grains were assumed to have the properties of quartz, E = 73.06 GPa (Young's modulus) and $\nu = 0.17$ (Poisson's ratio), and a friction coefficient f = 0.4. The three segments were generated using the equations in the text: loading path $0 \rightarrow A$ [Eq. (13)]; unloading path $A \rightarrow B$ [Eq. (14a)]; and reloading path $B \rightarrow C$ [Eq. (15a)].

where $K_3=(1-K_1f)/(2\ K_1f)$, and ε_{zz}^{**} is the strain at the point of reloading. Note that the reloading equation, Eq. (15a), degenerates to the loading equation, Eq. (13), when the points of unloading and reloading are the same, i.e., when $\varepsilon^{**}=\varepsilon^{*}$.

The stress–strain behavior predicted by these equations (Fig. 2) have the basic elements that are observed in laboratory stress–strain measurements on sandstones: nonlinearity, hysteresis, path-dependent moduli (i.e., note the presence of the strain history terms ε_{zz}^{*} and ε_{zz}^{**} in the stress–strain relations), and stress-induced anisotropy (for axisymmetric loading, the initially cubic sample becomes tetragonal).

3.2. Path-independence of the dynamic modulus

Using these equations, the volumetric strain can be decomposed into separate contributions resulting from nonlinear grain contact deformation and frictional slip compaction. First, consider the loading path $0 \rightarrow A$ (Fig. 2). An expression for the tangent moduli with friction completely locked-up can be obtained by noting that the grains are frictionally locked-up at the point of unloading, because the stored elastic strain in the material is insufficient to cause the grains to backslip. This can be seen by differentiating Eq. (14a) and setting $\varepsilon_{zz}=\varepsilon_{zz}^{*}$,

$$c_{33}^{\text{locked}}=\left.\frac{\mathrm{d}\sigma_{zz}^{\text{unload}}}{\mathrm{d}\varepsilon_{zz}}\right|_{\varepsilon_{zz}=\varepsilon_{zz}^{*}}=\left[\frac{\mu(4-3\nu)}{(1-\nu)(2-\nu)}\right]\varepsilon_{zz}^{*1/2}. \tag{16}$$

This expression is the dynamic uniaxial strain modulus which describes the velocity of compressional waves travelling along the z-axis $c_{\text{p}}=\sqrt{c_{33}^{\text{locked}}/\rho}$, where ρ is the density of the packing. An identical expression can be obtained for the unloading path $A \rightarrow B$ (Fig. 2) by differentiating Eq. (15a) and setting $\varepsilon_{zz}=\varepsilon_{zz}^{**}$,

$$c_{33}^{\text{locked}}=\left.\frac{\mathrm{d}\sigma_{zz}^{\text{reload}}}{\mathrm{d}\varepsilon_{zz}}\right|_{\varepsilon_{zz}=\varepsilon_{zz}^{**}}=\left[\frac{\mu(4-3\nu)}{(1-\nu)(2-\nu)}\right]\varepsilon_{zz}^{**1/2}. \tag{17}$$

The equivalence of Eqs. (16) and (17) and the dependence on only ε_{zz} indicate that the dynamic modulus for uniaxial strain loading is a path-independent function of the strain (Fig. 3).

Integrating the dynamic modulus, Eq. (16) or (17), along the loading path gives an expression for the stress–strain behavior resulting from nonlinearity only (i.e., without the effects of friction),

$$\sigma_{zz}^{\text{nonlin}}=\int_0^{\varepsilon_{zz}} c_{33}^{\text{locked}}\,\mathrm{d}\varepsilon_{zz}=\left[\frac{2\mu(4-3\nu)}{3(1-\nu)(2-\nu)}\right]\varepsilon_{zz}^{3/2}. \tag{18}$$

The value of the friction coefficient required to prevent intergranular slip (i.e., frictional lock-up) can be obtained by equating Eq. (18) with the loading Eq. (13) and solving for f,

$$f^{*}=\frac{2(1-\nu)}{(2-\nu)}. \tag{19}$$

Eq. (19) reveals that the coefficient of friction required to prevent intergranular slip increases as the Poisson's ratio of the grain is reduced (e.g., $f^{*}=0.85$ for $\nu=0.25$; $f^{*}=0.89$ for $\nu=0.20$). This value of the friction coefficient completely eliminates hysteresis in the stress–strain relations, resulting in a stress–strain curve with nonlinearity only. That is, the stress–strain curves for the loading and unloading paths collapse into one curve, as shown in Fig. 3, when $f=f^{*}$.

3.3. Decomposition of the volumetric strain

For a prescribed loading path, it is possible to decompose the volumetric strain into a path-independent contribution from nonlinear grain contact deformation and a path-dependent contribution from intergranular frictional slip compaction,

$$\varepsilon_{\text{b}}=\varepsilon_{zz}^{\text{nonlin}}+\varepsilon_{zz}^{\text{friction}}, \tag{20}$$

where from Eq. (18),

$$\varepsilon_{zz}^{\text{nonlin}}=\left[\frac{3(1-\nu)(2-\nu)}{2\mu(4-3\nu)}\right]^{2/3}\sigma_{zz}^{2/3}. \tag{21a}$$

Note that the volumetric strain ε_{b} is path-dependent because of the path-dependence of $\varepsilon_{zz}^{\text{friction}}$. For any uniaxial strain loading or unloading path, the path-inde-

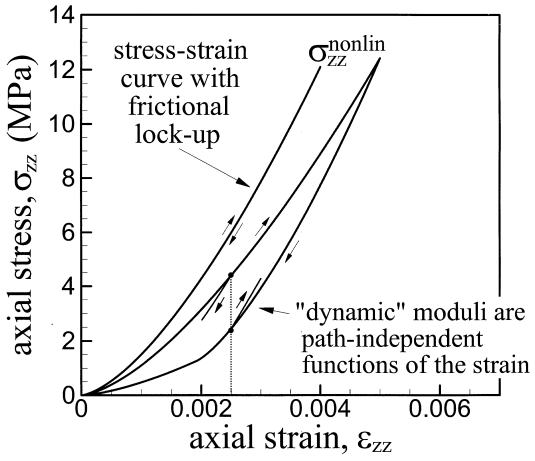

Fig. 3. Uniaxial strain $\sigma_{zz}^{\text{nonlin}}$ vs ε_{zz} curve for the fcc packing (properties are the same as in Fig. 2) with frictional lock-up ($f=f^{*}=0.91$) computed from Eq. (18). The uniaxial strain σ_{zz} vs ε_{zz} curve for a load–unload cycle [computed from Eqs. (13), (14a) and (14b)] is shown for reference. Small unloading and reloading excursions are also displayed on this curve [computed from Eqs. (14a) and (15a), respectively]. The equivalence of the slopes of these excursions indicates that the dynamic uniaxial strain modulus c_{33}^{locked} is a path-independent function of the axial strain.

pendent nonlinear contribution to the volumetric strain is given by Eq. (21a), and the path-dependent frictional slip contribution is the remainder. For example, the frictional slip contribution to the volumetric strain for the loading path can be obtained by subtracting Eq. (21a) from Eq. (13),

$$\varepsilon_{zz}^{\text{friction}}(\text{load}) = \left[\frac{3(1-\nu)}{2\mu(1+f)(4-3\nu)}\right]^{2/3} \times \{(4-3\nu)^{2/3} - [(2-\nu)(1+f)]^{2/3}\}\sigma_{zz}^{2/3}. \quad (21b)$$

An analogous expression for the frictional slip contribution to the volumetric strain along the unloading path, $\varepsilon_{zz}^{\text{friction}}(\text{unload})$, can also be obtained by (numerically) inverting the stress–strain relation given in Eq. (14) and subtracting out the nonlinear contribution given in Eq. (21a). In general, this expression will not be the same as Eq. (21b) (i.e., $\varepsilon_{zz}^{\text{friction}}(\text{load}) \neq \varepsilon_{zz}^{\text{friction}}(\text{unload})$, unless $f=f^*$) because of the path-dependence introduced by the intergranular frictional slip.

The nonlinear and frictional contributions to the volumetric strain for the loading path predicted by these relations [Eqs. (21a) and (21b)] are shown graphically in Fig. 4. The contribution of the frictional slip-assisted compaction $\varepsilon_{zz}^{\text{friction}}(\text{load})$ to the volumetric strain decreases as the friction coefficient is increased. As $f \to f^*$, the grains become frictionally locked-up and the frictional slip contribution [Eq. (21b)] approaches zero. At the other extreme, $f = 0$, the frictional slip contribution is largest, approaching 54% of the volumetric strain resulting from the nonlinear contribution $\varepsilon_{zz}^{\text{nonlin}}$.

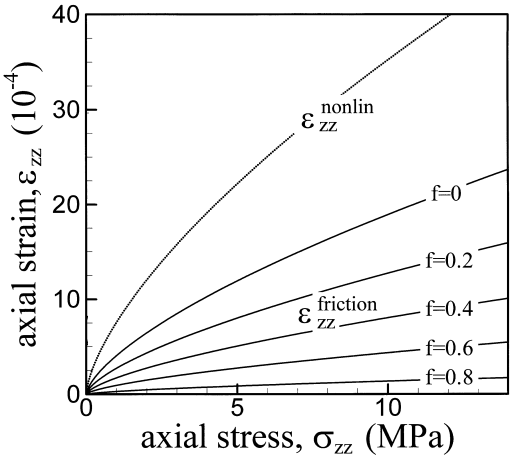

Fig. 4. Decomposition of the volumetric strain of the fcc packing for uniaxial strain conditions. The nonlinear contribution to the volumetric strain $\varepsilon_{zz}^{\text{nonlin}}$ computed using Eq. (21a) is displayed as a dotted curve. The frictional slip contribution to the volumetric strain computed for the loading path $\varepsilon_{zz}^{\text{friction}}(\text{load})$ using Eq. (21b) for a range of friction coefficients is shown as solid curves. Note that the frictional slip contribution approaches zero as $f \to f^* = 0.91$.

3.4. Ratio of the static to dynamic modulus

An additional result that can be obtained from the fcc model is the relationship between the *static* (i.e., large-strain tangent) and dynamic moduli. The uniaxial strain dynamic modulus is described by Eq. (16). The uniaxial strain static modulus for the loading path can be obtained by differentiating Eq. (13),

$$c_{33}^{\text{load}} = \frac{\mathrm{d}\sigma_{zz}^{\text{load}}}{\mathrm{d}\varepsilon_{zz}} = \left[\frac{\mu(1+f)}{(1-\nu)}\right]\varepsilon_{zz}^{1/2}. \quad (22)$$

Taking the ratio of Eqs. (22) and (16) gives the (path-dependent) ratio of the static-to-dynamic moduli for the loading path,

$$R^{\text{load}} = \left[\frac{c_{33}^{\text{load}}}{c_{33}^{\text{locked}}}\right] = \frac{(1+f)(2-\nu)}{(4-3\nu)}. \quad (23)$$

This ratio is a stress- and strain-independent function of the friction coefficient. As the friction coefficient is increased to the value required for frictional lock-up (i.e., $f \to f^*$), $R^{\text{load}} \to 1$ and the static and dynamic moduli become equivalent. It should be noted that Eq. (23) predicts a constant static-to-dynamic moduli ratio $R^{\text{load}} = 0.53$ for $\nu = 0.2$. In practice, this ratio is commonly observed to be stress-dependent. For example, Cheng and Johnston [3] reported $R^{\text{load}} \approx 0.4$–$0.9$ for Berea and Navajo sandstone subjected to sandstone stresses from 0–210 MPa. The results of the laboratory measurements on Berea sandstone described in the next section also show a stress-dependent R^{load} (Fig. 5). This difference is probably a result of the perfect symmetries of the fcc sphere packing which produces frictional sliding at all contacts over the entire loading path [12,24]. It appears likely that the disorder in the grain packing structure of sandstones is responsible for the observed smaller frictional lock-up at

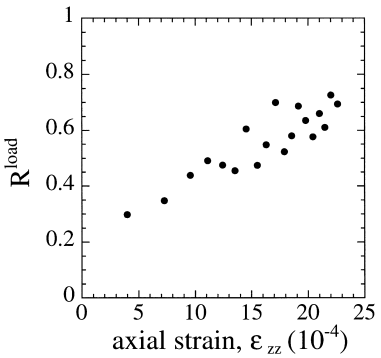

Fig. 5. R^{load} ratio of the static to dynamic uniaxial strain moduli c_{33} measured along the loading path on dry Berea sandstone.

lower stresses and greater frictional lock-up at higher stresses than that predicted by the simple fcc sphere packing model; however, presently, this behavior is not well understood.

4. Laboratory stress–strain measurements on Berea sandstone

In this section, we will use the results of laboratory stress–strain measurements on (dry) Berea sandstone to provide support of several of the findings of the previous section. Namely, for uniaxial strain consolidation in the reversible regime, we will show that: (1) the dynamic modulus is a path-independent function of the strain; and (2) the volumetric strain can be decomposed into path-independent nonlinear and path-dependent frictional slip components.

The uniaxial strain test was performed on a cylindrical sample of Berea sandstone (nominally isotropic, porosity = 0.22, density = 2.1 g/cc) 5.08 cm in diameter and 4.23 cm in length. The cylindrical surface of the sample was first spin-casted with a thin film of Wood's metal, a non-wetting, low melting point lead alloy (Cerrosafe®), then inserted into a plastic jacket (Fig. 6(a)). The Wood's metal coating served a dual purpose in providing a smooth surface onto which the radial strain gauge could be attached and to minimize

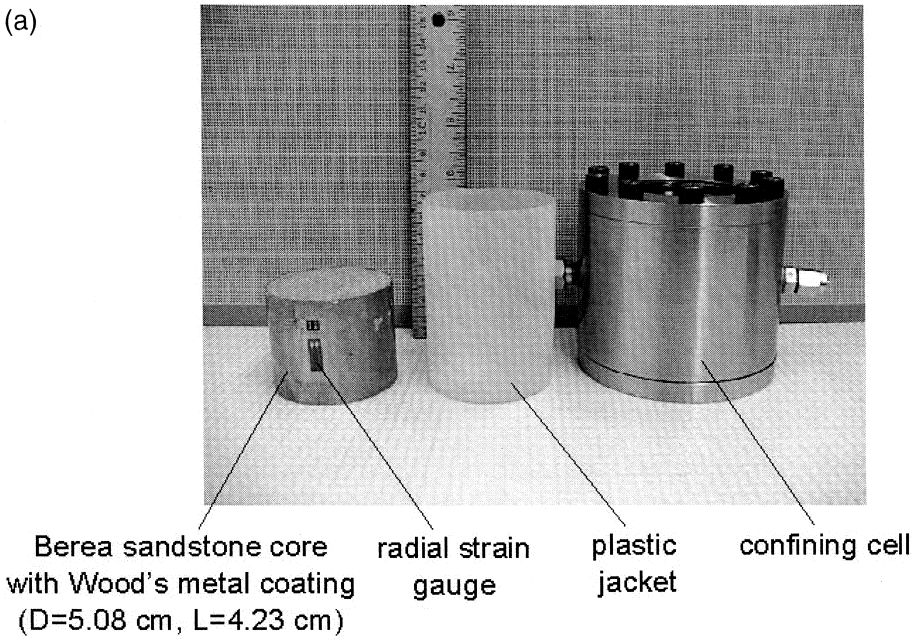

Fig. 6. (a) Photograph of the Wood's metal jacketed Berea sandstone sample (diameter = 5.08 cm; length = 4.23 cm), plastic jacket, and confining cell used in the uniaxial strain tests. (b) Schematic of the experimental set-up for the uniaxial strain tests on dry Berea sandstone. Radial strain was monitored with a strain gauge bonded to the Wood's metal surface. Axial displacement was measured with two linear variable displacement transducers (LVDTs), axial load with a load cell, and radial stress with a pressure transducer. P-wave velocities were measured with ultrasonic transducers located on the ends of the sample. Uniaxial strain conditions were maintained by adjusting the confining pressure to maintain zero radial strain.

the intrusion of the plastic jacket into the porous sides of the rock. The jacketed sample was inserted into a confining vessel, and the assembly was placed in a load frame with a load cell to measure the axial stress, two linear variable displacement transducers (LVDTs) to measure the axial displacement, a pressure transducer to measure the radial stress, and two ultrasonic transducers (1 MHz) to measure the P-wave velocity (Fig. 6(b)). All tests were performed on oven dried samples. As the sample was subjected to increasing axial stress, the radial strain was monitored and the confining pressure was increased accordingly to maintain a condition of zero radial strain (i.e., uniaxial strain conditions).

4.1. Path-independence of the dynamic modulus

A typical stress–strain curve from the test is displayed in Fig. 8. During the major loading and unloading paths, ultrasonic P-wave velocities were measured at regular intervals. The elastic modulus computed from the P-wave velocities provide direct estimates of the uniaxial strain dynamic modulus c_{33}^{locked} (i.e., $c_{33}^{\text{locked}} = \rho c_{\text{p}}^2$). The plot of c_{33}^{locked} obtained from the P-wave velocities for the loading and unloading paths indicates that c_{33}^{locked} is a path-independent function of the strain (compare Fig. 7(a) and (b)). Numerical integration of these moduli with respect to strain [analogous to Eq. (16) for the fcc packing] along the loading and unloading paths produces a new stress–strain relation that describes only the nonlinear contribution to the overall volumetric strain (Fig. 8; analogous to Fig. 3 for the fcc packing),

$$\sigma_{zz}^{\text{nonlin}} = \int_0^{\varepsilon_{zz}} c_{33}^{\text{locked}}\, \mathrm{d}\varepsilon_{zz}. \tag{24}$$

Because the frictional component of the deformation has been removed, this stress–strain curve has a higher tangent modulus and lacks hysteresis between loading and unloading. The same process outlined here should yield the same stress–strain relation when applied to any loading or unloading path provided that c_{33}^{locked} is a path-independent function of the strain, as appears to be the case for the uniaxial strain loading and unloading paths.

4.2. Decomposition of the volumetric strain

An estimate of the frictional slip contribution to the volumetric strain of Berea sandstone for the uniaxial strain loading path can be obtained from Eq. (20),

$$\varepsilon_{zz}^{\text{friction}} = \varepsilon_{\text{b}} - \varepsilon_{zz}^{\text{nonlin}}. \tag{25}$$

The procedure for obtaining the strain–stress relations for ε_{b} and $\varepsilon_{zz}^{\text{nonlin}}$ from the measured axial stress–strain and P-wave velocity data is straightforward if it is assumed that the initially isotropic sample will exhibit transverse stress-induced anisotropy (TI) when subjected to uniaxial strain loading along the z-axis. For

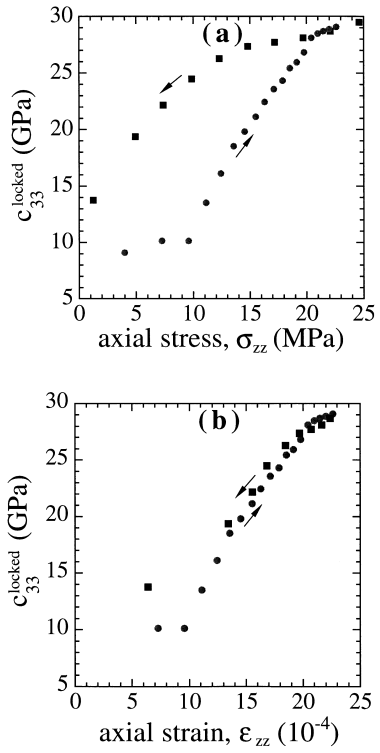

Fig. 7. Dynamic uniaxial strain moduli c_{33}^{locked} computed from the P-wave velocities measured in Berea sandstone ($c_{33}^{\text{locked}} = \rho c_{\text{p}}^2$, where ρ is the density and c_{p} is the P-wave velocity): (a) c_{33}^{locked} vs σ_{zz}; and (b) c_{33}^{locked} vs ε_{zz}. The lack of hysteresis between the loading and unloading parts of c_{33}^{locked} when plotted as a function of the axial strain suggests that the dynamic moduli are path-independent functions of the strain.

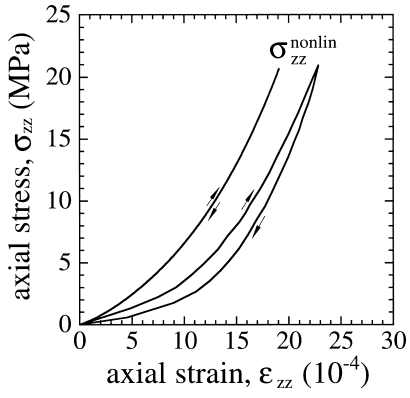

Fig. 8. $\sigma_{zz}^{\text{nonlin}}$ vs ε_{zz} curve for Berea sandstone under uniaxial strain conditions obtained by fitting a curve to the c_{33}^{locked} vs ε_{zz} data in Fig. 7(b) and numerically integrating Eq. (28). The uniaxial strain σ_{zz} vs ε_{zz} curve for a load–unload cycle is shown for reference.

uniaxial strain conditions, the strain–stress relations for a TI material take the following simplified form,

$$d\varepsilon_{zz} = 2s_{13}\, d\sigma_{rad} + s_{33}\, d\sigma_{zz} \tag{26}$$

$$d\varepsilon_{rad} = (s_{11} + s_{12})d\sigma_{rad} + s_{13}\, d\sigma_{zz} = 0$$

$$\rightarrow d\sigma_{rad} = -\left(\frac{s_{13}}{s_{11} + s_{12}}\right)d\sigma_{zz}, \tag{27}$$

where $d\varepsilon_{rad} \equiv d\varepsilon_{xx} = d\varepsilon_{yy}$ and $d\sigma_{rad} \equiv d\sigma_{xx} = d\sigma_{yy}$. Substituting Eq. (27) into Eq. (26) yields the following equation for the axial strain in terms of only the axial stress

$$d\varepsilon_{zz} = \left(s_{33} - \frac{2s_{13}^2}{s_{11} + s_{12}}\right)d\sigma_{zz} \rightarrow d\varepsilon_{zz} = s_{zz}\, d\sigma_{zz}. \tag{28}$$

Comparison of Eq. (28) with the uniaxial strain stress–strain relation for a TI material,

$$d\sigma_{zz} = c_{33}\, d\varepsilon_{zz}, \tag{29}$$

reveals that $s_{zz} = c_{33}^{-1}$. Thus, for uniaxial strain loading on a sample which exhibits TI stress-induced anisotropy, the axial strain–stress relation can be obtained by numerical integration of Eq. (28) with $s_{zz} = c_{33}^{-1}$, where c_{33} is obtained from P-wave velocities measured at points along the loading path ($c_{33}^{locked} = \rho c_p^2$) for the estimate of $\varepsilon_{zz}^{nonlin}$, and c_{33} is the tangent modulus $c_{33} = d\sigma_{zz}/d\varepsilon_{zz}$ measured along the loading path for the estimate of ε_b.

The decomposition of the volumetric strain into its nonlinear and frictional contributions [Eq. (25)], using the procedure described above, is displayed graphically in Fig. 9. The decomposition reveals that the frictional contribution to the volumetric strain of Berea sandstone for uniaxial strain loading is largest at low stresses (40%, Fig. 10). However, even at the higher stresses, the frictional contribution accounts for as much as 20% of the total volumetric strain.

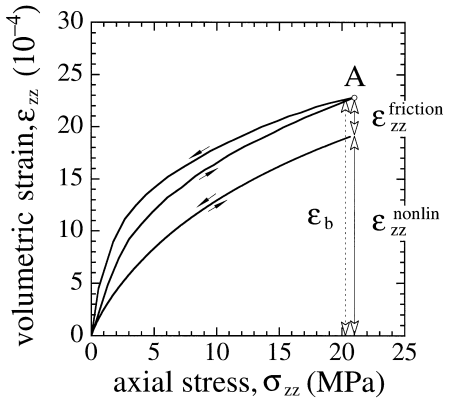

Fig. 9. Graphical decomposition of the volumetric strain $\varepsilon_b (= \varepsilon_{zz})$ of dry Berea sandstone into contributions from frictional slip-assisted compaction (path-dependent) $\varepsilon_{zz}^{friction}$ and nonlinear grain contact deformation (path-independent) $\varepsilon_{zz}^{nonlin}$ for the loading path $0 \rightarrow A$.

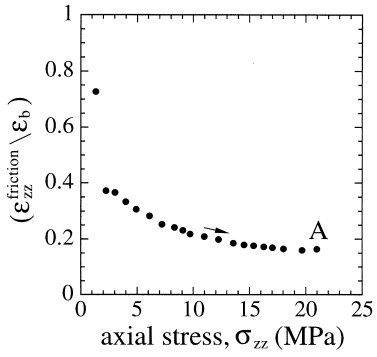

Fig. 10. Frictional contribution $\varepsilon_{zz}^{friction}$ to the total volumetric strain ε_b for the loading path shown in Fig. 9.

5. Summary and conclusions

Frictional slip along grain contacts is a well-known mechanism for pore volume reduction and dilation in soils. This study has demonstrated that similar processes may occur in a medium porosity sandstone. Using the analytic results for the stress–strain behavior of a face-centered cubic sphere packing with Hertz–Mindlin contact mechanics, we demonstrated that for uniaxial strain consolidation, the dynamic modulus is a path-independent function of the strain. We also showed that it is possible to decompose the volumetric strain into a path-independent contribution from nonlinear grain contact deformation and a path-dependent contribution from frictional slip compaction. Laboratory stress–strain measurements on Berea sandstone were demonstrated to be consistent with this finding and, in addition, revealed that frictional slip compaction accounts for a significant portion of the volumetric strain of Berea sandstone for uniaxial strain loading.

The results of this study highlight the importance of considering frictional effects when attempting to evaluate the volumetric strain of sandstone. For the specific conditions of this study (i.e., uniaxial strain loading, unloading, and reloading paths), friction slip between grains was shown to result in a path-dependent volumetric strain [e.g., $\varepsilon_b(\sigma_{ij}$; path $A) \neq \varepsilon_b(\sigma_{ij}$; path $B)$; note that Norris and Johnson [21] and Johnson et al. [16] demonstrate that a random sphere pack subjected to different loading paths exhibits path-dependence even in the absence of frictional slip). However, for these conditions, the nonfrictional part of the volumetric strain can be extracted by integration of the path-independent, dynamic moduli obtained from seismic velocity measurements made at different static

loads. Additional work is needed to determine both the magnitude and character of the path-dependence of the volumetric strain and the anisotropic elastic moduli of sandstones, and to determine if the analysis presented here can be extended to general three-dimensional loading.

Acknowledgements

The authors would like to thank Ziqiong Zheng and Laura Pyrak-Nolte for enlightening discussions on the mechanical properties of unconsolidated rock. This research was funded by the Director, Office of Energy Research, Office of Basic Energy Sciences, under US Department of Energy Contract No. DE-AC03-76SF00098.

Appendix. Derivation of the reloading stress–strain relations

The procedures for obtaining the loading and unloading uniaxial strain stress–strain relations for the face centered cubic (fcc) packing of identical spheres with Hertz–Mindlin contact mechanics [Eqs. (13) and (14), respectively] are described by Hendron [12] and Stoll [24], respectively. Here, we provide the essential steps for developing the reloading axial stress–strain relations [Eq. (15)].

The ingredients for the derivation are the equations describing the normal and tangential compliances, the equation of equilibrium, the compatibility condition, the normal contact force–displacement relation, and the strain–force relation:

normal compliance (from Hertz theory)

$$C = \frac{\mathrm{d}\alpha}{\mathrm{d}N} = \frac{1-\nu}{2\mu a}, \quad \text{where } a = \left[\frac{3(1-\nu)RN}{8\mu}\right]^{1/3}, \tag{A1}$$

tangential compliance for the reloading path [24] [Eq. (19)]

$$S = \frac{\mathrm{d}\delta}{\mathrm{d}T} = \frac{2-\nu}{4\mu a}\left[f\frac{\mathrm{d}N}{\mathrm{d}T} + \left(1 - f\frac{\mathrm{d}N}{\mathrm{d}T}\right) \times \left(1 + \frac{T^{**} - T}{2fN} + \frac{N^{**} - N}{2N}\right)^{-1/3}\right], \tag{A2}$$

equation of equilibrium [24] [Eq. (9)]

$$\mathrm{d}N + \mathrm{d}T = \sqrt{2}R^2\sigma_{zz}, \tag{A3}$$

compatibility condition [24] [Eq. (10)]

$$\mathrm{d}\delta - \mathrm{d}\alpha = 0, \tag{A4}$$

normal contact force–displacement relation [24] [Eq. (11)]

$$\mathrm{d}\alpha = C\,\mathrm{d}N, \tag{A5}$$

normal strain–force relation [24] [Eq. (12)]

$$\mathrm{d}\varepsilon_{zz} = \frac{C}{R}\mathrm{d}N, \tag{A6}$$

where Eqs. (A3)–(A6) are specific to an fcc packing subjected to axisymmetric loading in the z-direction (Fig. 1). The variables which appear in these equations are defined as follows:

- a radius of the circular area of contact between identical spheres
- f coefficient of sliding friction
- N magnitude of the normal contact force acting between spheres with contacts oriented at 45° to the z-axis (Fig. 1)
- R sphere radius
- T magnitude of the tangential contact force acting between spheres with contacts oriented at 45° to the z-axis (Fig. 1)
- α relative approach between spheres with centers oriented at 45° to the z-axis (Fig. 1)
- δ relative tangential displacement between spheres with centers oriented at 45° to the z-axis (Fig. 1)
- μ shear modulus of the sphere
- ν Poisson's ratio of the sphere.

The tangential compliance for the reloading path given in Eq. (A2) can be recast into an expression relating the tangential and normal contact forces using Eqs. (A1), (A4), and (A5),

$$\frac{\mathrm{d}N}{\mathrm{d}T} = \frac{2-\nu}{2(1-\nu)}\left[f\frac{\mathrm{d}N}{\mathrm{d}T} + \left(1 - f\frac{\mathrm{d}N}{\mathrm{d}T}\right) \times \left(1 + \frac{T^{**} - T}{2fN} + \frac{N^{**} - N}{2N}\right)^{-1/3}\right]. \tag{A7}$$

After some algebraic manipulations, Eq. (A7) can be recast into a form which can be integrated from the initial point of reloading (N^{**}, T^{**}) to a point on the reloading curve (N, T). This integration produces the following equation which describes the tangential contact force at any point on the reloading curve

$$T = T^{**} - 2f\left\{[(1+K_3)N^{**}2/3 - K_3N^{2/3}]^{3/2} - \frac{(N+N^{**})}{2}\right\}, \tag{A8}$$

where $K_3=(1-K_1f)/(2K_1f)$ with $K_1=(2-\nu)/[2(1-\nu)]$. Here, T^{**} is the tangential contact force at the point of reloading which can be obtained from the unloading equation developed by Stoll [24] [Eq. (17)]

$$T^{**} = T^* + 2f\left\{[(1+K_2)N^{*2/3} - K_2N^{2/3}]^{3/2} - \frac{(N+N^*)}{2}\right\}, \tag{A9}$$

where $K_2=-(1+K_1f)/(2\ K_1f)$ and $T^*=fN^*$ is the tangential contact force at the point of unloading [24] [Eq. (13)].

The axial stress–strain relation for the reloading curve is obtained by integrating the equation of equilibrium (A3) from the unloaded state (0, 0) to the current state on the reloading curve (N, T)

$$\int_0^{\sigma_{zz}} \mathrm{d}\sigma_{zz} = \frac{1}{\sqrt{2}R^2}\left(\int_0^N \mathrm{d}N + \int_0^T \mathrm{d}T\right) \rightarrow \sigma_{zz} = \frac{1}{\sqrt{2}R^2}(N+T). \tag{A10}$$

Substitution of Eq. (A9) into Eq. (A10) gives

$$\sigma_{zz} = \frac{1}{\sqrt{2}R^2}\{(1+f\ )N + 2f[(1+K_2)N^{*2/3} - K_2N^{**}2/3]^{3/2} - 2f[(1+K_3)N^{**2/3} - K_3N^{2/3}]^{3/2}\}. \tag{A11}$$

The normal contact force N can be replaced by the axial strain ε_{zz} by substituting Eq. (A1) into Eq. (A6) and integrating from zero load to the point on the reloading curve

$$N = \frac{2^{3/2}\mu R^2}{3(1-\nu)}\varepsilon_{zz}^{3/2}. \tag{A12}$$

Substitution of Eq. (A12) into Eq. (A11) gives the axial stress–strain relations for the reloading path [Eq. (15); segment $B\rightarrow C$ in Fig. 2)

$$\sigma_{zz}^{\text{reload}} = \left[\frac{2\mu}{3(1-\nu)}\right]\{(1+f\ )\varepsilon_{zz}^{3/2} + 2f[(1+K_2)\varepsilon_{zz}^{*} - K_2\varepsilon_{zz}^{**}]^{3/2} - 2f[(1+K_3)\varepsilon_{zz}^{**} - K_3\varepsilon_{zz}]^{3/2}\}, \quad \text{for } [(1+K_2)\varepsilon_{zz}^{*} - K_2\varepsilon_{zz}^{**}] \geq 0 \tag{A13a}$$

$$\sigma_{zz}^{\text{reload}} = \left[\frac{2\mu}{3(1-\nu)}\right]\{(1+f\ )\varepsilon_{zz}^{3/2} - 2f[(1+K_3)\varepsilon_{zz}^{**} - K_3\varepsilon_{zz}]^{3/2}\}, \quad \text{for } [(1+K_2)\varepsilon_{zz}^{*} - K_2\varepsilon_{zz}^{**}] < 0. \tag{A13b}$$

References

[1] Chen WF, Mizuno E. Nonlinear analysis in soil mechanics. In: Developments in Geotechnical Engineering, vol. 53. Amsterdam: Elsevier Science, 1990 672 pp.

[2] Chang CS, Chang Y, Kabir MG. Micromechanics modeling for stress–strain behavior of granular soils. I. Theory. J Geotech Eng 1992;118:1959–74.

[3] Cheng CH, Johnston DH. Dynamic and static moduli. Geophys Res Lett 1981;8(1):39–42.

[4] Cook NGW, Hodgson K. Some detailed stress–strain curves for rock. J Geophys Res 1965;70(12):2883–8.

[5] Deresiewicz H. Stress–strain relations for a simple model of a granular medium. J Appl Mech 1958;25:402–6.

[6] Duffy J. A differential stress–strain relation for the hexagonal close-packed array of elastic spheres. J Appl Mech 1959;26:88–94.

[7] Duffy J, Mindlin RD. Stress–strain relations and vibrations of a granular medium. J Appl Mech 1957;24:585–93.

[8] Elata D, Berryman JG. Contact force–displacement laws and the mechanical behavior of random packs of identical spheres. Mech of Mat 1996;24:229–40.

[9] Guyer RA, McCall KR, Boitnott GN. Hysteresis, discrete memory, and nonlinear wave propagation in rock: a new paradigm. Phys Rev Lett 1995;74(17):3491–4.

[10] Guyer RA, McCall KR, Boitnott GN, Hilbert Jr LB, Plona TJ. Quantitative implementation of Preisach–Mayergoyz space to find static and dynamic elastic moduli in rock. J Geophys Res 1997;102:5281–93.

[11] Guyer RA, Johnson PA. Nonlinear mesoscopic elasticity: evidence for a new class of materials. In: Physics today, 1999 30–36 April.

[12] Hendron AJ. The behavior of sand in one-dimensional compression. Ph.D. thesis, University of Illinois, Urbana/Champaign, IL, 1963.

[13] Hilbert Jr LB, Hwong TK, Cook NGW, Nihei KT, Myer LR. Effects of strain amplitude on the static and dynamic nonlinear deformation of Berea sandstone. In: Nelson, Laubach, editors. Rock mechanics. Rotterdam: Balkema, 1994. p. 487–504.

[14] Jaeger JC, Cook NGW. Fundamentals of rock mechanics. 3rd ed. New York: Chapman and Hall, 1979 593 pp.

[15] Johnson PA, Rasolofosaon PNJ. Nonlinear elasticity and stress-induced anisotropy in rock. J Geophys Res 1996;101:3113–24.

[16] Johnson DL, Schwartz LM, Elata D, Berryman JG, Hornby B, Norris AN. Linear and nonlinear elasticity of granular media: stress-induced anisotropy of a random sphere pack. J Appl Mech 1998;65:380–8.

[17] Lo T, Coyner KB, Toksöz MN. Experimental determination of elastic anisotropy of Berea sandstone, Chicopee shale, and Chelmsford granite. Geophys 1986;51:164–71.

[18] McCall KR, Guyer RA. Equation of state and wave propagation in hysteretic nonlinear elastic materials. J Geophys Res 1994;99:23,887–97.

[19] Mindlin RD. Compliance of elastic bodies in contact. J Appl Mech 1949;16:259–68.

[20] Mindlin RD, Deresiewicz H. Elastic spheres in contact under varying oblique forces. J Appl Mech 1953;24:585–93.
[21] Norris AN, Johnson DL. Nonlinear elasticity of granular media. J Appl Mech 1997;64:39–49.
[22] Nur A, Simmons G. Stress-induced velocity anisotropy in rock: an experimental study. J Geophys Res 1969;74(27):6667–74.
[23] Ruistuen H, Teufel LW. Analysis of the influence of stress path on the compressibility of weakly cemented sandstones using laboratory experiments and discrete particle models. In: Aubertin, Hassani and Mitri editors. Rock mechanics. Amsterdam: Balkema, 1996. p. 1525–31.
[24] Stoll RD. Stress-induced anisotropy in sediment acoustics. J Acoust Soc Am 1989;85(2):702–8.
[25] Thurston CW, Deresiewicz H. Analysis of a compression test of a model of a granular medium. J Appl Mech 1959;26:251–8.
[26] Walton K. The effective elastic moduli of a random packing of spheres. J Mech Phys Solids 1987;35:213–26.
[27] Zheng Z. Compressibility of porous rocks under different stress conditions. Int J Rock Mech Min Sci and Geomech Abstr 1993;30(7):1181–4.
[28] Zimmerman RW. Compressibility of sandstone. In: Development in petroleum science, vol. 29. Amsterdam: Elsevier Science, 1991 173 pp.